RADAR CONSTRAINTS ON THE THICKNESS OF SUBSURFACE ICE NEAR HELLAS PLANITIA, MARS. C. W. Cook[1], A. M. Bramson[1], M. S. Christoffersen[2], S. Byrne[1], J. W. Holt[1], D. Viola[3], C. M. Dundas[4], T. A. Goudge[2], [1]Lunar and Planetary Laboratory, University of Arizona, Tucson, AZ 85721 (clairec@email.arizona.edu), [2]Jackson School of Geosciences, University of Texas, Austin, TX 78758, [3]NASA Ames Research Center, Mountain View, CA 94035, [4]U.S. Geological Survey, Astrogeology Science Center, 2255 N. Gemini Dr., Flagstaff, AZ 86001

Introduction: The presence and nature of subsurface ice in the mid-latitudes of Mars has implications for the planet's climate history. Variations in obliquity and eccentricity drive changes in insolation that lead to the transfer of water molecules around Mars [1]. Although water ice is currently unstable on the surface of Mars at the mid-latitudes, it is possible that relatively pure "excess ice" resides in the subsurface [2], having been deposited on the surface under different climatic conditions.

Scalloped depressions [3–5], expanded craters [4–6], pedestal craters [7], lobate debris aprons (LDAs) [8], and banded terrain [9], are geomorphological features potentially related to the presence of subsurface ice that are present in and around Hellas Planitia, a region in the southern mid-latitudes of Mars. Previous estimates of the thickness of an ice-rich mantle in parts of Malea Planum and Hellas basin are between 13 and 39 m [10], and estimates for the southern hemisphere as a whole yield a thickness of 15 m [11]. However, several scarps exposing mid-latitude ice sheets found between 55–60°S are at least 130 m thick [12].

The Shallow Radar (SHARAD) instrument on the Mars Reconnaissance Orbiter (MRO) can detect dielectric interfaces associated with subsurface layers that are at least 10–20 m thick [13] so SHARAD may be able to identify the base of an ice layer in Hellas Planitia.

Methods: We surveyed 368 SHARAD tracks covering the entirety of Hellas Planitia and some surrounding areas. Candidate reflectors were identified by examining radargrams, which depict delay time versus distance along the spacecraft's track, with the power returned at each pixel represented by its brightness. Reflections from off-nadir topographic features ("clutter") may appear at time delays similar to subsurface reflections. Therefore, we compared the radargrams to simulations based on Mars Orbiter Laser Altimeter (MOLA) topography data [14].

We categorized potential reflectors based on properties that affected our confidence that they are due to real subsurface returns. The "low confidence" categories are as follows. LC1 refers to reflectors that are contiguous with returns visible in the clutter simulation. LC2 refers to reflectors that are curved. LC3 is for reflectors that are both contiguous with clutter and curved. LC4 is for reflectors which appear at similar locations as possible clutter, but are much brighter. The LC5 category is for reflectors that closely match the shape and size of nearby clutter. LC6 is for reflectors that appear to correspond to clutter whose positions are shifted slightly from where they are expected in the simulations. We deemed reflectors lacking the qualities described above to be of higher confidence.

Additionally, we tested the higher-confidence reflectors with higher-resolution clutter simulations based on HRSC and CTX Digital Terrain Models (DTMs), which can show features missing in the coarser MOLA clutter simulations.

We used CTX images near the higher-confidence reflectors and the HiRISE survey of [4] to identify geomorphology potentially indicative of subsurface ice, (scalloped depressions, expanded craters, pedestal craters, LDAs, and banded terrain) within 20 km of these reflectors. For reflectors identified near these potentially ice-related features, we measured the one-way delay time, Δt, between surface and subsurface reflectors and converted it to a depth of the subsurface radar return, Δx, assuming a given dielectric constant (ε_r) using $\Delta x = \frac{c\Delta t}{\sqrt{\varepsilon_r}}$ where c is the speed of light. For reflectors found near scalloped depressions, expanded craters, and pedestal craters, we constrained the range of depths to the reflectors assuming a composition that ranges from pure ice, $\varepsilon_r = 3.15$ [15], to dense basalt, $\varepsilon_r = 8$ [16].

We used ArcGIS tools to perform a hot-spot analysis on the higher-confidence reflectors to identify any statistically significant clustering, using a similar workflow as in [4].

Results: By comparison of the radargrams to the MOLA clutter simulations, we initially identified 601 candidate radar reflectors, with higher confidence in 193 (a map of the candidate reflectors is shown in Figure 1). However, most of the candidate reflectors, including those in which we otherwise have higher confidence, are short along-track (86% are < 10 km) and often lack a counterpart in adjacent tracks, which lowers our confidence that these reflectors correspond to real subsurface interfaces. We checked 40 candidate reflectors categorized as high confidence using cluttersims derived from HRSC DTMs and found that 67.5% clearly appeared to be clutter in the HRSC simulations, which supports the idea that many of the candidate reflectors identified overall are likely clutter from unresolved topography. The CTX DTMs generally had too little overlap with the SHARAD tracks to be useful due to day/night track orientations, but one CTX cluttersim contained a feature matching a candidate radar reflector.

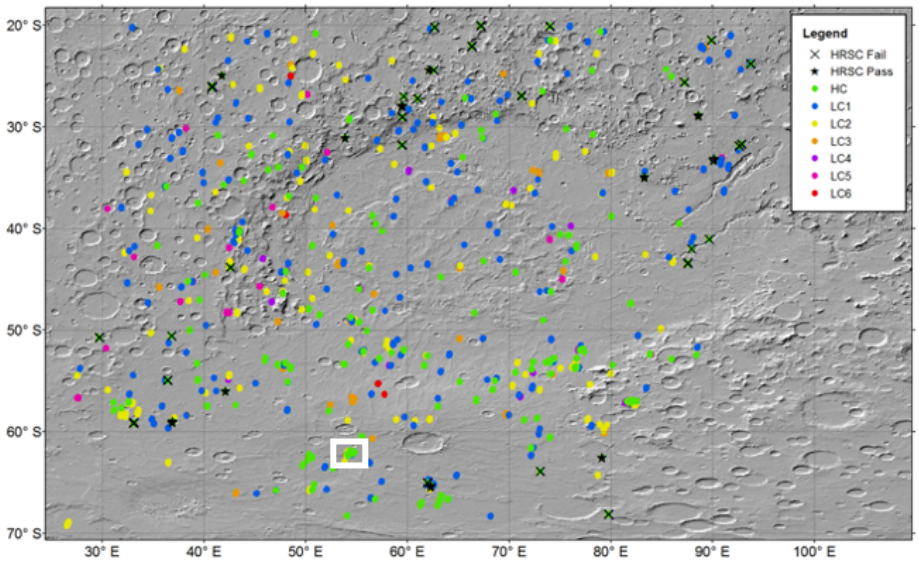

Figure 1: Map of candidate subsurface radar reflectors. Colored dots mark candidate reflectors. An X marks reflectors that correspond to clutter in HRSC clutter simulations, a star marks reflectors that do not correspond to clutter in HRSC clutter simulations. The white box marks the location of Figure 2.

If we assume an icy composition with $\varepsilon_r = 3.15$, the median depths of the reflectors near scalloped depressions and expanded craters are 95 m and 131 m, respectively (these depths are within a standard deviation of each other). Assuming a composition of $\varepsilon_r = 8$, the median depths of the reflectors near scalloped depressions and expanded craters are 60 m and 82 m, respectively.

We have especially high confidence in a group of six adjacent reflectors associated with layering within a mound in Malea Patera. The reflectors have a median depth of 89 m assuming ε_r=3.15 and a median depth of 56 m assuming ε_r=8. Three of the reflectors are similar in shape to the surface reflector (but do not follow it exactly and have a greater time delay than would be expected for radar sidelobes [17]), and appear as though they could be due to material draping some underlying topography (two are shown in Figure 2). There are scalloped depressions on top of the mound, within 20 km of all but one of the reflectors, and a scarp at the edge which exposes layering.

We also identified several reflectors associated with an LDA. We created depth-corrected radargrams by converting the vertical axis from time-delay to depth assuming dielectric constants of 3.15 and 8, and found that $\varepsilon_r = 3.15$ results in a basal reflector that is approximately horizontal and aligned with the surrounding surface reflector, as expected for a basal interface. This dielectric constant indicates an ice-rich composition.

We did not find any high confidence candidate reflectors associated with banded terrain.

The results of the hot spot analysis indicate a statistically significant concentration of reflectors around 50–60°S, similar to the hot spot for expanded craters in the region [4].

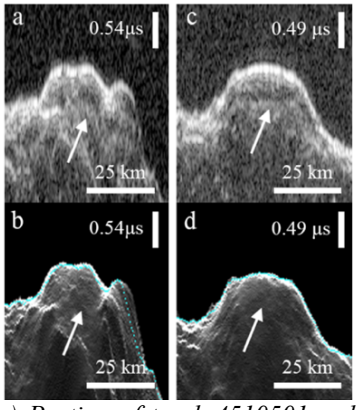

Figure 2: a) Portion of track 4510501 radargram, b) corresponding clutter simulation for (a), c) portion of track 4554702 radargram, d) corresponding clutter simulation for (c).

References: [1] Head J. W. et al. (2003) *Nature 426*, 797-802. [2] Mellon M.T. et al. (2004) *Icarus, 169,* 324–340. [3] Zanetti M. et al. (2010) *Icarus, 206*, 691-706. . [4] Viola D. and McEwen A. S. (2018), *JGR, 123*, 262-277. [5] Dundas C. M. et al. (2015) *Icarus, 262*, 154-169. [6] Viola D. et al. (2015) *Icarus, 248*, 190-204. [7] Kadish S. et al. (2008) *GRL, 35*, L16104. [8] Holt J. et al. (2008) *Science, 322*, 1235-1238. [9] Diot X. et al. (2015), *JGR, 120*, 2258–2276 [10] Zanetti M. et al. (2009) *LPSC XL,* Abstract #2365. [11] Levy J. et al. (2018) *JGR, 123, 322-334*. [12] Dundas C. et al. (2018) *Science, 359*, 199-201. [13] Seu R. et al. (2007) *JGR, 112*, E05S05. [14] Choudary P. (2016) *IEEE GRSL, 13*, 9, 1285-1289. [15] Matsuoka T. et al. (1997) *J. Phys. Chem. B, 101,* 6219-6222. [16] Rust A. et al. (1999) *JVGR, 91,* 79-96. [17] Putzig N.E. et al. (2014) *JGR, 119,* 1936-1949.